VIP Core–Shell Nanostructures Very Important Paper

Deutsche Ausgabe: DOI: 10.1002/ange.201507176
Internationale Ausgabe: DOI: 10.1002/anie.201507176

Energy Migration Upconversion in Manganese(II)-Doped Nanoparticles

Xiyan Li, Xiaowang Liu, Daniel M. Chevrier, Xian Qin, Xiaoji Xie, Shuyan Song, Hongjie Zhang, Peng Zhang,* and Xiaogang Liu**

Dedicated to Professor Guangxian Xu

Abstract: *We report the synthesis and characterization of cubic $NaGdF_4$:Yb/Tm@$NaGdF_4$:Mn core–shell structures. By taking advantage of energy transfer through Yb→Tm→Gd→Mn in these core–shell nanoparticles, we have realized upconversion emission of Mn^{2+} at room temperature in lanthanide tetrafluoride based host lattices. The upconverted Mn^{2+}emission, enabled by trapping the excitation energy through a Gd^{3+} lattice, was validated by the observation of a decreased lifetime from 941 to 532 μs in the emission of Gd^{3+} at 310 nm ($^6P_{7/2}$→ $^8S_{7/2}$). This multiphoton upconversion process can be further enhanced under pulsed laser excitation at high power densities. Both experimental and theoretical studies provide evidence for Mn^{2+} doping in the lanthanide-based host lattice arising from the formation of F^- vacancies around Mn^{2+} ions to maintain charge neutrality in the shell layer.*

Since the discovery of the phenomenon of upconversion in the mid-1960s,[1] tremendous success has been achieved with respect to elucidating fundamental optical mechanisms, identifying optimal host–dopant combinations for efficient upconversion processes, and precisely controlling emission profiles.[2] As a unique class of luminescent phosphors, upconversion nanocrystals hold great promise in a broad range of applications spanning from bioimaging through drug delivery to 3D volumetric display.[3] Despite the notable achievements over the past decade, efficient photon upconversion is almost exclusively restricted to lanthanide activators. A formidable challenge is the development of upconversion nanocrystal systems dominated by transition-metal-activated emission.

The generation of photon upconversion through transition-metal ions is important for expanding the scope of upconversion nanocrystals in favor of diverse applications in lighting, molecular sensing, and photovoltaics.[4] Previously, several attempts have been made to realize upconversion emission by using transition-metal ions such as Mn^{2+}, Ni^{2+}, and Cr^{3+}.[5] However, the investigation of optical properties typically has to be carried out at cryogenic temperatures[5,6] or in perovskite/magnetoplumbite host lattices.[7]

Recently, our research group has demonstrated efficient anti-Stokes emission by an energy migration process for a variety of lanthanide activators without long-lived intermediate energy states.[8] The realization of tunable anti-Stokes emissions by energy migration through Gd sublattice provides insights into the rational design of luminescent materials that display unprecedented properties. We reason that the effect of the energy migration on long-distance energy transfer can be harnessed to achieve photon upconversion for transition-metal ions with electronic sublevels within the $^6P_{7/2}$ level of Gd^{3+}.[9]

The experimental design is presented in Figure 1. We intended to synthesize a core–shell nanostructure in the form of $NaGdF_4$:Yb/Tm@$NaGdF_4$:Mn. A set of lanthanide or

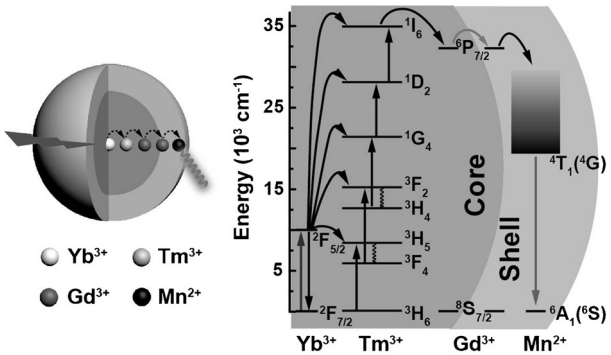

Figure 1. Illustration (left) and proposed energy transfer mechanism (right) of the Mn^{2+}-activated core–shell upconversion nanoparticles. Note that the core and shell regions are featured in different shades, and the energy transfer occurs through the Yb→Tm→Gd→Mn pathway in the core–shell nanoparticles upon 980 nm excitation.

[*] Dr. X. Li, X. Liu, Dr. X. Xie, Prof. X. Liu
Department of Chemistry, National University of Singapore
3 Science Drive 3, Singapore 117543 (Singapore)
E-mail: chmlx@nus.edu.sg
Dr. X. Qin, Prof. X. Liu
Institute of Materials Research and Engineering
Agency for Science, Technology and Research (A*STAR)
3 Research Link, Singapore 117602 (Singapore)
D. M. Chevrier, Prof. P. Zhang
Department of Chemistry, Dalhousie University
Halifax, Nova Scotia, B3H 4J3 (Canada)
E-mail: peng.zhang@dal.ca
Dr. S. Song, Prof. H. Zhang
State Key Laboratory of Rare Earth Resource Utilization
Changchun Institute of Applied Chemistry
Chinese Academy of Sciences
Changchun, Jilin 130022 (P. R. China)
E-mail: hongjie@ciac.ac.cn
Supporting information and ORCID(s) from the author(s) for this article are available on the WWW under http://dx.doi.org/10.1002/anie.201507176.

transition-metal ions (Yb^{3+}, Tm^{3+}, Gd^{3+}, Mn^{2+}) are incorporated into different core/shell layers to effectively eliminate deleterious cross-relaxation. The energy transfer to Mn^{2+} ions is enabled by a five-photon upconversion process to populated the high-lying $^1I_6$ state of Tm^{3+}, followed by energy migration through the Gd^{3+} sublattice at its excited $^6P_{7/2}$ state.

In a typical experiment, cubic $NaGdF_4$ nanocrystals 10 nm in size were first synthesized by a well-established thermal decomposition method (see the Supporting Information).[10] Upon epitaxial growth of a $NaGdF_4$:Mn (4 mol%) shell, the average size of the nanocrystals increased to around 12.5 nm (Figure 2a and Figure S1 in the Supporting Information). High-resolution transmission electron microscopy (HRTEM) imaging revealed the single-crystalline nature of the core–shell nanocrystals, as evidenced by the observation of clear lattice fringes with a measured *d*-spacing of 0.317 nm (inset of Figure 2a), which is in good agreement with the lattice spacing in the (111) planes of cubic-phase $NaGdF_4$. The high crystallinity and phase purity of the as-synthesized nanocrystals were also verified by powder X-ray diffraction (XRD) measurements (Figure 2b and Figure S2).

To confirm the incorporation of Mn^{2+} ions into the shell layer of the nanoparticles, we carried out X-ray absorption near-edge structure (XANES) and extended X-ray absorption fine structure (EXAFS) measurements. The Mn K-edge XANES of the core–shell structure shows the absorption edge position of Mn, which is in good agreement with that of divalent MnO (Figure 2c and Figure S3), thus suggesting an oxidation state of +2 for the Mn doped into the shell layer.[11] According to EXAFS fitting results (Figure 2d, Figure S3, and Table S1), the average first-shell Mn–F coordination number (CN) for Mn^{2+} ions is around 6, which is lower than that of Gd^{3+} ions (CN = 8) for the first-shell of Gd–F scattering. The reduced coordination number provides evidence for the formation of F^- vacancies in the crystal lattice in order to compensate for the charge imbalance upon replacement of Gd^{3+} with Mn^{2+} ions. To further verify our hypothesis, we performed density functional theory (DFT) based first-principles calculations on the formation energy of Mn-doped $NaGdF_4$ nanoparticles (Figure 2e).[12] We found that the replacement of Gd^{3+} with Mn^{2+} requires less energy than the substitution of Na^+ by Mn^{2+} ions. Moreover, the formation energy upon replacement of Gd^{3+} with Mn^{2+} ions further decreased to approximately 0.56 eV when a fluoride vacancy (V_F) was introduced at the first coordination shell to balance the charge discrepancy between Gd^{3+} and Mn^{2+} ions. The

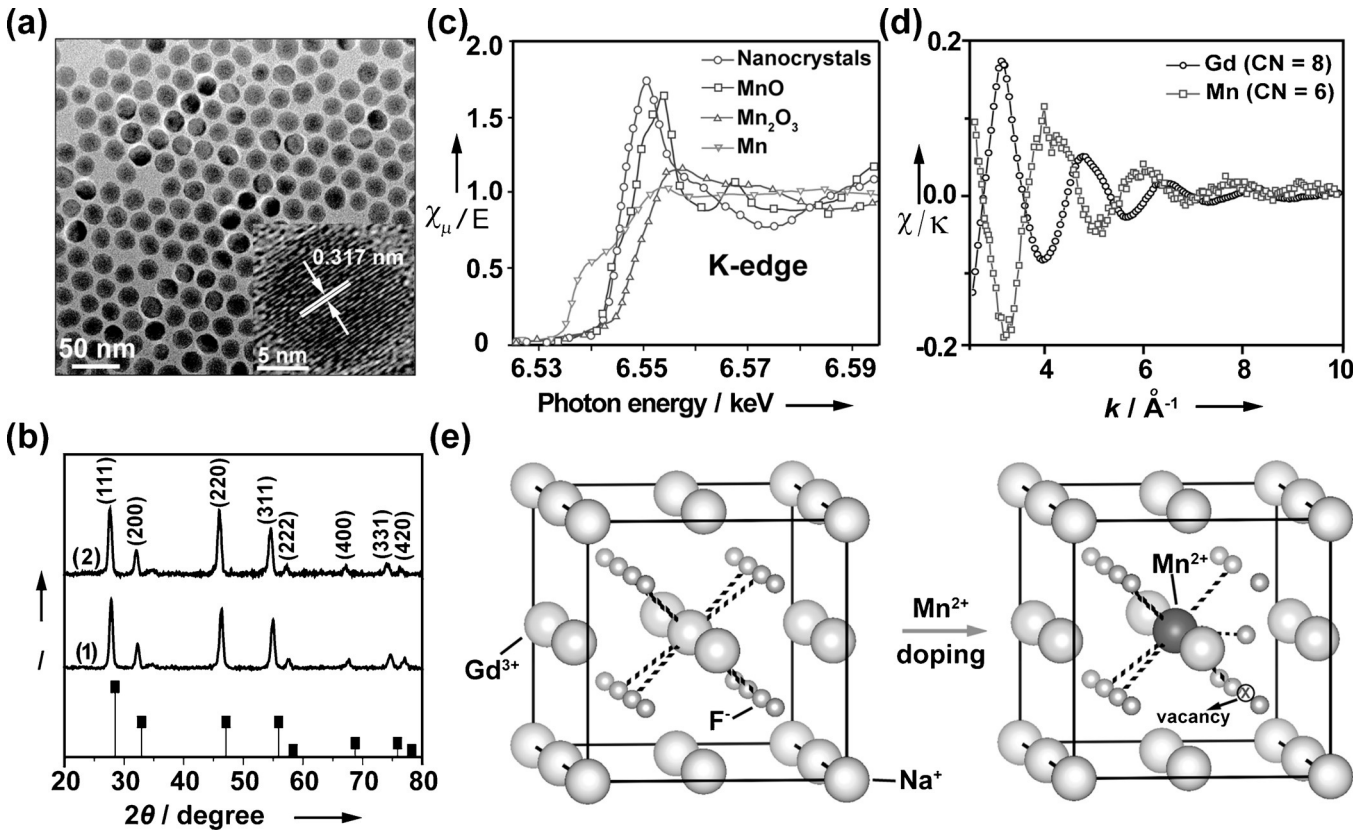

Figure 2. Structural characterization of the $NaGdF_4$:Yb/Tm@$NaGdF_4$:Mn nanoparticles. a) TEM image of the as-synthesized nanoparticles (inset: HRTEM image of a single-crystalline nanoparticle). b) XRD patterns of the as-synthesized 1) $NaGdF_4$:Yb/Tm@$NaGdF_4$ and 2) $NaGdF_4$:Yb/Tm@$NaGdF_4$:Mn nanoparticles, as indexed against the standard diffraction patterns of cubic $NaYbF_4$ crystals (Joint Committee on Powder Diffraction Standards file number 27-1426). c) Mn K-edge XANES spectra recorded for $NaGdF_4$:Yb/Tm@$NaGdF_4$:Mn nanoparticles, MnO, Mn_2O_3, and Mn metal, respectively. d) Experimental Gd L_3-edge and Mn K-edge EXAFS in k-space for $NaGdF_4$:Yb/Tm@$NaGdF_4$:Mn nanoparticles. e) Schematic presentation of $NaGdF_4$ crystal structures without and with Mn^{2+} dopant ions. Note that upon substitution of Gd^{3+} with Mn^{2+} ions, F^- vacancies may be introduced for maintaining the charge neutrality, thus resulting in a decrease in the coordination number of the Mn^{2+} ions.

calculation implies that the Mn^{2+} lattice structure can be stabilized by fluoride vacancies formed in the vicinity, consistent with the EXAFS characterization (Figure 2d).

The selection of a cubic $NaGdF_4$ matrix for realizing the upconverted emission of Mn^{2+} is due to the ease of accommodating Mn^{2+} ions into the cubic host lattice.[13] Note that no emission from Mn^{2+} was detectable when hexagonal-phase $NaGdF_4$:Yb/Tm was exploited as the core material for $NaGdF_4$:Mn shell passivation (Figure S4). Inductively coupled plasma atomic emission spectroscopy (ICP-AES) analysis revealed the absence of Mn^{2+} in the resulting nanoparticles. This result can be ascribed to the incompatibility of Mn^{2+} ions to the hexagonal phase host lattice.

Next, we investigated the luminescence properties of the $NaGdF_4$:Yb/Tm@$NaGdF_4$:Mn nanoparticles under excitation at 980 nm using a continuous-wave (CW) laser. Interestingly, a broad emission band centered at 535 nm was observed, in addition to the emission peaks from Tm^{3+} and Gd^{3+} (Figure 3a). We attributed the emission band at 535 nm to Mn^{2+} activation arising from its $^4T_1 \rightarrow {}^6A_1$ optical transition. As a result the Mn^{2+} emission, we observed a subtle change, under identical experimental conditions, in emission color from blue to light green when compared with that of the core–shell counterpart without the Mn^{2+} dopants (Figure 3a, inset). The Mn^{2+} emission lifetime from the core–shell nanoparticles was determined to be approximately 30 ms (Figure S5), much longer than that obtained at cryogenic temperatures.[5,6] This long lifetime of emission stems from the spin-forbidden nature of the $^4T_1 \rightarrow {}^6A_1$ transition.[14]

Intriguingly, we found that when irradiated with a high-power pulsed laser (3.8 ns, ca. 10^8 W cm^{-1}) the emission intensity of the Mn^{2+}-doped core–shell nanoparticles at 535 nm can be substantially increased (Figure 3a, 3), as evidenced by the observation of a visible green emission. Notably, the emission intensities at 290 and 311 nm from Tm^{3+} and Gd^{3+} ions, respectively, also increased under the pulsed laser excitation (Figure 3a). According to the power-dependent measurements (Figure 3b), the respective emissions of Mn^{2+}, Gd^{3+}, and Tm^{3+} at 535, 290, and 311 nm are likely to be governed by a five-photon process, which can be manipulated by varying the power density of the excitation laser. In our system, with the pumping of a 980 nm pulsed laser at a power density of 10^8 W cm^{-1}, the co-doping of Mn^{2+} with Gd^{3+} and Tm^{3+} clearly resulted in emission enhancement at 290 and 311 nm (Figure 3a and Figure S6).

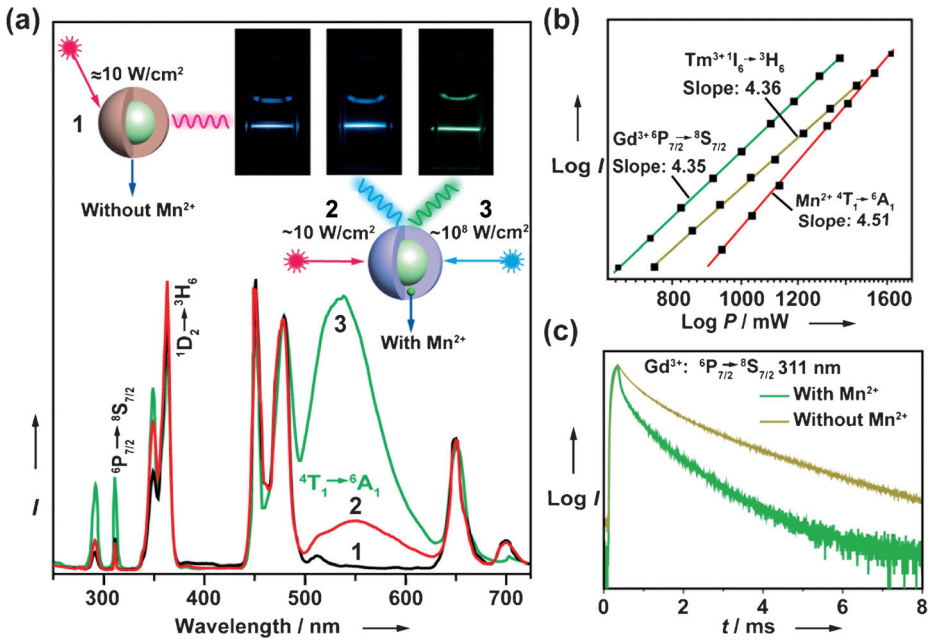

Figure 3. a) Upconversion emission profiles of 1) $NaGdF_4$:Yb/Tm@$NaGdF_4$ and 2) $NaGdF_4$:Yb/Tm@$NaGdF_4$:Mn nanoparticles recorded at room temperature under 980 nm CW excitation as well as 3) $NaGdF_4$:Yb/Tm@$NaGdF_4$:Mn nanoparticles irradiated with a pulsed OPO laser at a power density of 10^8 W cm^{-2}. The corresponding luminescence photos taken from cyclohexane solutions of the nanoparticles are inset. b) Log–log plots of the upconversion emission against the excitation power at 980 nm for $^6P_{7/2} \rightarrow {}^8S_{7/2}$ transition of Gd^{3+}, $^1I_6 \rightarrow {}^3H_6$ transition of Tm^{3+}, and $^4T_1 \rightarrow {}^6A_1$ transition of Mn^{2+}. c) A comparison of upconversion lifetimes of Gd^{3+} in $NaGdF_4$:Yb/Tm@$NaGdF_4$:Mn and $NaGdF_4$:Yb/Tm@$NaGdF_4$ nanoparticles. Note that the core–shell nanoparticles used in the time-decay measurement were pretreated with concentrated HCl to remove the surface oleate ligands that may quench the upconversion emission at around 300 nm.

To confirm the energy transfer from Gd^{3+} to Mn^{2+}, we performed time-decay measurements of the Gd^{3+} and Tm^{3+} emission (Figure 3c and Figure S7). A notable decrease in the lifetime of the Gd^{3+} emission at 311 nm from 941 to 532 μs was observed upon Mn^{2+} doping in the shell layer, while the lifetimes of Tm^{3+} at different energy levels remained virtually unaltered. Additionally, we found that the emission of Mn^{2+} is sensitive to the Gd^{3+} content doped in the core. For instance, on increasing the doping concentration of Y^{3+} from 2 to 10 mol%, the emission of Mn^{2+} gradually decreased and then eventually disappeared (Figure S8). Taken together, these results unambiguously demonstrate the dominant role of Gd^{3+} lattices in regulating the upconverted emission of Mn^{2+}.

The spatially confined doping of Yb^{3+}, Tm^{3+}, and Mn^{2+} ions into respective core and shell layers is another important factor in generating intense emission of Mn^{2+}. In the case of $NaGdF_4$:Yb/Tm/Mn nanoparticles without the core–shell structure, we observed comparably weak Mn^{2+} emission (Figure S9). Even in the presence of an inert shell of $NaYF_4$ on the triply doped $NaGdF_4$:Yb/Tm/Mn nanoparticles, the emission was considered to be weak as a result of deleterious relaxation between Tm^{3+} and Mn^{2+}. Similar to previously reported results,[15] the energy migration upconversion in Mn^{2+}-doped nanoparticles

is also strongly influenced by the doping concentration. For example, the optimal doping concentration of core is 49:1 mol% for Yb^{3+}/Tm^{3+}, consistent with our previous reports (Figure S10, S11).[8a] The strongest upconversion emission was achieved with an Mn^{2+} dopant content of 4.4 mol% as measured by ICP-AES (Figure S12, S13). There is a large discrepancy in the Mn^{2+} dopant content between the experimental results and theoretical estimation, mainly because of the low reactivity of the Mn^{2+} precursor during the synthetic process (Table S2).[16]

To further enhance the upconversion emission of Mn^{2+}, an effective approach is to grow an inert shell onto $NaGdF_4$:Yb/Tm@$NaGdF_4$:Mn nanoparticles as the trapping of the excitation energy from Gd^{3+} by Mn^{2+} competes with the vibration-induced nonradiative process caused by surface quenchers.[8b] As anticipated, we observed a marked increase in Mn^{2+} emission upon passivating the nanoparticles with a thin layer of $NaYF_4$ (Figure S14). In contrast, only a weak enhancement in the emission was observed when $NaGdF_4$ was introduced as the shell layer. This behavior can be best explained by the migration of the excitation energy through the Gd^{3+} sublattice to surface quenching sites.[8]

The realization of photon upconversion in Mn^{2+}-doped core–shell nanoparticles permits the investigation of energy transfer between transition metal and lanthanide ions, and this study potentially leads to an enriched color output. For example, on doping a combination of Mn^{2+} and Tb^{3+} (15 mol%) into the shell layer of $NaGdF_4$:Yb/Tm@$NaGdF_4$:Mn/Tb nanoparticles, we observed emissions from both activators (Figure S15). By comparison, the emission band of Mn^{2+} disappeared when Tb^{3+} were substituted with Eu^{3+} (15 mol%), thus indicating the occurrence of efficient energy transfer from the Mn^{2+} to Eu^{3+} ions.[17] However, the energy transfer from Mn^{2+} to Eu^{3+} can be prevented by inserting an extra layer to separate the Eu^{3+} from Mn^{2+} ions (Figure S15).

Given the strong tendency for Mn^{2+} ions to undergo oxidation, the as-prepared $NaGdF_4$:Yb/Tm@$NaGdF_4$:Mn nanoparticles allow for the development of a sensing platform for small molecules. As a proof of concept, we recorded the emission profile of colloidal solutions of ligand-free $NaGdF_4$:Yb/Tm@$NaGdF_4$:Mn nanoparticles in the presence of different amounts of H_2O_2 (Figure 4).[18] It was found that the intensity of the Mn^{2+} emission decreased gradually with increasing H_2O_2 content, while the emission profile of Tm^{3+} was not affected (Figure 4b). The quenching of the Mn^{2+} emission could be ascribed to Mn^{2+} oxidation at the particle surface by the H_2O_2 oxidant.[17] Interestingly, with the coating of an inert $NaYF_4$ layer onto the $NaGdF_4$:Yb/Tm@$NaGdF_4$:Mn nanoparticles, the Mn^{2+} emission was unperturbed by H_2O_2, even at a high concentrations (16 M; Figure S16, S17).

The ability of Mn^{2+}-doped upconversion nanoparticles to sense H_2O_2 may provide a luminescent probe for real-time monitoring H_2O_2 generation in a variety of biological processes.[18,19] This hypothesis was validated by adding glucose oxidase to $NaGdF_4$:Yb/Tm@$NaGdF_4$:Mn nanoparticles. In the presence of H_2O and O_2, glucose oxidase can selectively catalyze the conversion of D-glucose into gluconic acid, accompanied by the generation of H_2O_2 as a side product. Our preliminary result exhibited a reduction in the emission intensity of Mn^{2+} at 535 nm with increasing levels of glucose oxidase (Figure S18).

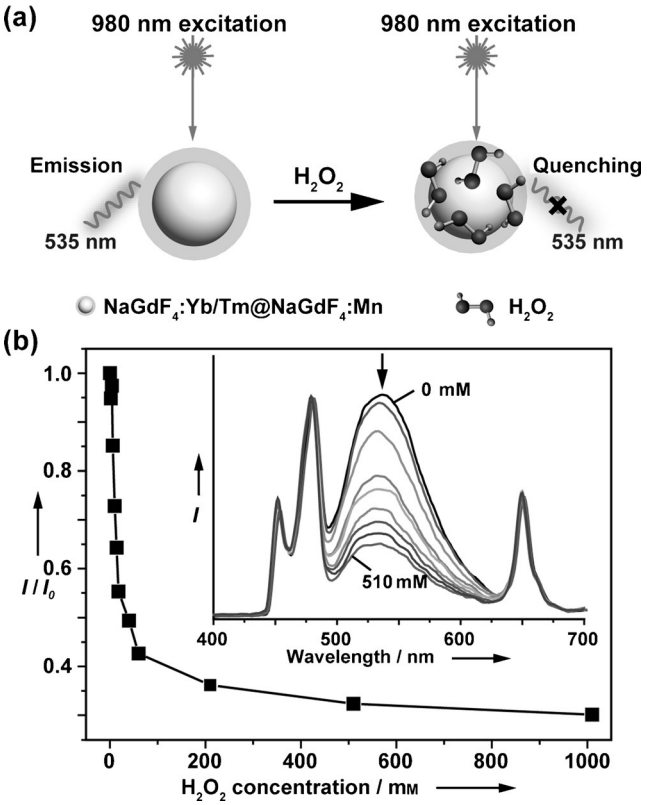

Figure 4. a) H_2O_2 sensing by using $NaGdF_4$:Yb/Tm@$NaGdF_4$:Mn nanoparticles. In the presence of H_2O_2 molecules, the upconverted emission of Mn^{2+} from the core–shell nanoparticles at 535 nm can be suppressed by the oxidation of Mn^{2+} by H_2O_2. b) Emission intensity dependence (as measured by the ratio of I/I_o at 535 nm) on H_2O_2 concentration (0, 2, 6, 10, 14, 40, 60, 210, and 510 mM). The change in the upconversion emission spectrum as a function of H_2O_2 concentration added to the particle solution is shown as inset. The spectra were obtained by irradiating the solution with a pulsed OPO laser to minimize the thermal heating effect. Note that the core–shell nanoparticles used in this study were pretreated with concentrated HCl to afford ligand-free particles readily dispersible in aqueous solutions.

In conclusion, our investigations illustrate that transition metal ions such as Mn^{2+} can play a role in photon upconversion. From our perspective, the optimal design of the core–shell nanostructure and Gd^{3+}-mediated energy migration might prove to be the most critical for realizing upconversion emission through Mn^{2+} activation. The color output of the as-prepared colloidal solutions can be readily tuned from whitish-blue to bright green by varying the power density of the excitation source. The readily oxidizable nature of Mn^{2+} ions make these nanoparticles amenable to hydrogen peroxide detection. These findings would provide new insights into the design of an optical sensing platform useful for monitoring oxidation process in biological systems.

Acknowledgements

The work was supported in part by the Singapore Ministry of Education (grant no. MOE2010-T2-1-083), the Agency for Science, Technology and Research (A*STAR; grant no. 1231AFG028), and the National Natural Science Foundation of China (grant nos. 51173081, 61136003, and 21210001). P.Z. acknowledges funding support from NSERC Canada. The Canadian Light Source (CLS) is supported by NSERC Canada, CIHR, NRC and the University of Saskatchewan. PNC/XSD facilities (Sector 20) at the Advanced Photon Source (APS) are supported by the U.S. DOE, NSERC Canada, the University of Washington, the CLS, and the APS. Use of the APS is supported by the U.S. DOE under contract no. DE-AC02-06CH11357.

Keywords: doping · lanthanides · nanoparticles · transition metals · upconversion

How to cite: *Angew. Chem. Int. Ed.* **2015**, *54*, 13312–13317
Angew. Chem. **2015**, *127*, 13510–13515

[1] F. Auzel, *C. R. Seances Acad. Sci. Ser. B* **1966**, *262*, 1016–1019.

[2] a) M. Haase, H. Schäfer, *Angew. Chem. Int. Ed.* **2011**, *50*, 5808–5829; *Angew. Chem.* **2011**, *123*, 5928–5950; b) X. Liu, C.-H. Yan, J. A. Capobianco, *Chem. Soc. Rev.* **2015**, *44*, 1299–1301; c) M.-K. Tsang, G. Bai, J. Hao, *Chem. Soc. Rev.* **2015**, *44*, 1585–1607; d) H. H. Gorris, R. Ali, S. M. Saleh, O. S. Wolfbeis, *Adv. Mater.* **2011**, *23*, 1652–1655; e) L.-D. Sun, Y.-F. Wang, C.-H. Yan, *Acc. Chem. Res.* **2014**, *47*, 1001–1009; f) J. Hao, Y. Zhang, X. Wei, *Angew. Chem. Int. Ed.* **2011**, *50*, 6876–6880; *Angew. Chem.* **2011**, *123*, 7008–7012; g) X. Chen, D. Peng, Q. Ju, F. Wang, *Chem. Soc. Rev.* **2015**, *44*, 1318–1330; h) X. Liu, R. Deng, Y. Zhang, Y. Wang, H. Chang, L. Huang, X. Liu, *Chem. Soc. Rev.* **2015**, *44*, 1479–1508; i) L. Tu, X. Liu, F. Wu, H. Zhang, *Chem. Soc. Rev.* **2015**, *44*, 1331–1345; j) M. Bettinelli, *Nat. Nanotechnol.* **2015**, *10*, 203–204; k) E. M. Chan, G. Han, J. D. Goldberg, D. J. Gargas, A. D. Ostrowski, P. J. Schuck, B. E. Cohen, D. J. Milliron, *Nano Lett.* **2012**, *12*, 3839–3845; l) X. Ye, J. Chen, M. Engel, J. A. Millan, W. Li, L. Qi, G. Xing, J. E. Collins, C. R. Kagan, J. Li, S. C. Glotzer, C. B. Murray, *Nat. Chem.* **2013**, *5*, 466–473; m) X. Li, F. Zhang, D. Zhao, *Chem. Soc. Rev.* **2015**, *44*, 1346–1378; n) N. J. J. Johnson, A. Korinek, C. Dong, F. C. J. M. van Veggel, *J. Am. Chem. Soc.* **2012**, *134*, 11068–11071; o) H. Schäfer, P. Ptacek, O. Zerzouf, M. Haase, *Adv. Funct. Mater.* **2008**, *18*, 2913–2918; p) H. Schäfer, C. Hess, H. Tobergte, A. Volf, S. Ichilmann, H. Eickmeier, B. Voss, N. Kashaev, J. Nordmann, W. Akram, B. H. -Azanza, M. Steinhart, *Small* **2015**, *11*, 931–935; q) S. Schietinger, L. D. Menezes, B. Lauritzen, O. Benson, *Nano Lett.* **2009**, *9*, 2477–2481; r) S. Schietinger, T. Aichele, H.-Q. Wang, T. Nann, O. Benson, *Nano Lett.* **2010**, *10*, 134–138; s) J. Wang, T. Ming, Z. Jin, J. Wang, L.-D. Sun, C.-H. Yan, *Nat. Commun.* **2014**, *5*, 5669.

[3] a) R. Deng, F. Qin, R. Chen, W. Huang, M. Hong, X. Liu, *Nat. Nanotechnol.* **2015**, *10*, 237–242; b) G. Chen, H. Qiu, P. N. Prasad, X. Chen, *Chem. Rev.* **2014**, *114*, 5161–5214; c) N. M. Idris, M. K. G. Jayakumar, A. Bansal, Y. Zhang, *Chem. Soc. Rev.* **2015**, *44*, 1449–1478; d) D. Yang, P. Ma, Z. Hou, Z. Cheng, C. Li, J. Lin, *Chem. Soc. Rev.* **2015**, *44*, 1416–1448; e) Y. Sun, W. Feng, P. Yang, C. Huang, F. Li, *Chem. Soc. Rev.* **2015**, *44*, 1509–1525; f) Y. Min, J. Li, F. Liu, E. K. L. Yeow, B. Xing, *Angew. Chem. Int. Ed.* **2014**, *53*, 1012–1016; *Angew. Chem.* **2014**, *126*, 1030–1034; g) L. Cheng, K. Yang, Q. Chen, Z. Liu, *ACS Nano* **2012**, *6*, 5605–5613; h) X. Bai, D. Li, Q. Liu, B. Dong, S. Xu, H. Song, *J. Mater. Chem.* **2012**, *22*, 24698–24704; i) J. Wang, T. Wei, X. Li, B. Zhang, J. Wang, C. Huang, Q. Yuan, *Angew. Chem. Int. Ed.* **2014**, *53*, 1616–1620; *Angew. Chem.* **2014**, *126*, 1642–1646; j) L.-L. Li, R. Zhang, L. Yin, K. Zheng, W. Qin, P. R. Selvin, Y. Lu, *Angew. Chem. Int. Ed.* **2012**, *51*, 6121–6125; *Angew. Chem.* **2012**, *124*, 6225–6229; k) K. Zheng, Z. Liu, C. Lv, W. Qin, *J. Mater. Chem. C* **2013**, *1*, 5502–5507; l) Z. Chen, Z. Liu, Z. Li, E. Ju, N. Gao, L. Zhou, J. Ren, X. Qu, *Biomaterials* **2015**, *39*, 15–22; m) H. H. Gorris, O. S. Wolfbeis, *Angew. Chem. Int. Ed.* **2013**, *52*, 3584–3600; *Angew. Chem.* **2013**, *125*, 3668–3686; n) Q. Liu, Y. Sun, T. Yang, W. Feng, C. Li, F. Li, *J. Am. Chem. Soc.* **2011**, *133*, 17122–17125; o) Z. Li, S. Lv, Y. Wang, S. Chen, Z. Liu, *J. Am. Chem. Soc.* **2015**, *137*, 3421–3427; p) Y. Xiao, L. Zeng, T. Xia, Z. Wu, Z. Liu, *Angew. Chem. Int. Ed.* **2015**, *54*, 5323–5327; *Angew. Chem.* **2015**, *127*, 5413–5417.

[4] a) J. F. Suyver, A. Aebischer, D. Biner, P. Gerner, J. Grimm, S. Heer, K. W. Krämer, C. Reinhard, H. U. Güdel, *Opt. Mater.* **2005**, *27*, 1111–1130; b) R. Martin-Rodriguez, R. Valiente, F. Rodriguez, F. Piccinelli, A. Speghini, M. Bettinelli, *Phys. Rev. B* **2010**, *82*, 075117.

[5] a) P. Gerner, C. Reinhard, H. U. Güdel, *Chem. Eur. J.* **2004**, *10*, 4735–4741; b) O. S. Wenger, R. Valiente, H. U. Güdel, *Phys. Rev. B* **2001**, *64*, 235116; c) S. Ye, Y.-j. Li, D.-C. Yu, G.-P. Dong, Q.-Y. Zhang, *J. Mater. Chem.* **2011**, *21*, 3735–3739; d) J. Grimm, O. S. Wenger, H. U. Güdel, *J. Lumin.* **2003**, *102*, 380–385; e) S. Heer, K. Petermann, H. U. Güdel, *J. Lumin.* **2003**, *102*, 144–150.

[6] a) C. Reinhard, P. Gerner, R. Valiente, O. S. Wenger, H. U. Güdel, *J. Lumin.* **2001**, *94*, 331–335; b) C. Reinhard, P. Gerner, F. Rodriguez, S. Garcia-Revilla, R. Valiente, H. U. Güdel, *Chem. Phys. Lett.* **2004**, *386*, 132–136; c) P. Gerner, C. Fuhrer, C. Reinhard, H. U. Güdel, *J. Alloys Compd.* **2004**, *380*, 39–44.

[7] a) E.-H. Song, S. Ding, M. Wu, S. Ye, F. Xiao, G.-P. Dong, Q.-Y. Zhang, *J. Mater. Chem. C* **2013**, *1*, 4209–4215; b) E. H. Song, S. Ding, M. Wu, S. Ye, Z. T. Chen, Y. Y. Ma, Q. Y. Zhang, *Opt. Mater. Express* **2014**, *4*, 1186–1196; c) E. Song, S. Ding, M. Wu, S. Ye, F. Xiao, S. Zhou, Q. Zhang, *Adv. Opt. Mater.* **2014**, *2*, 670–678.

[8] a) F. Wang, R. R. Deng, J. Wang, Q. X. Wang, Y. Han, H. M. Zhu, X. Y. Chen, X. G. Liu, *Nat. Mater.* **2011**, *10*, 968–973; b) Q. Su, S. Han, X. Xie, H. Zhu, H. Chen, C.-K. Chen, R.-S. Liu, X. Chen, F. Wang, X. Liu, *J. Am. Chem. Soc.* **2012**, *134*, 20849–20857.

[9] a) P. Liu, G. Zhou, J. Zhang, S. Chen, Y. Yang, S. Wang, *J. Lumin.* **2013**, *144*, 57–63; b) Y. Tanabe, S. Sugano, *J. Phys. Soc. Jpn.* **1954**, *9*, 753–766.

[10] a) M. M. Lage, R. L. Moreira, F. M. Matinaga, J.-Y. Gesland, *Chem. Mater.* **2005**, *17*, 4523–4529; b) H.-X. Mai, Y.-W. Zhang, R. Si, Z.-G. Yan, L.-d. Sun, L.-P. You, C.-H. Yan, *J. Am. Chem. Soc.* **2006**, *128*, 6426–6436; c) J.-C. Boyer, F. Vetrone, L. A. Cuccia, J. A. Capobianco, *J. Am. Chem. Soc.* **2006**, *128*, 7444–7445; d) X. Li, R. Wang, F. Zhang, L. Zhou, D. Shen, C. Yao, D. Zhao, *Sci. Rep.* **2013**, *3*, 3536; e) J. Shen, G. Chen, A. M. Vu, W. Fan, O. S. Bilsel, C. C. Chang, G. Han, *Adv. Opt. Mater.* **2013**, *1*, 644–650.

[11] J. H. Barkyoumb, A. N. Mansour, *Phys. Rev. B* **1992**, *46*, 8768–8776.

[12] S. J. Clark, M. D. Segall, C. J. Pickard, P. J. Hasnip, M. I. Probert, K. Refson, M. C. Payne, *Z. Kristallogr.* **2005**, *220*, 567–570.

[13] a) G. Tian, Z. J. Gu, L. J. Zhou, W. Y. Yin, X. X. Liu, L. Yan, S. Jin, W. L. Ren, G. M. Xing, S. J. Li, Y. L. Zhao, *Adv. Mater.* **2012**, *24*, 1226–1231; b) S. Zeng, Z. Yi, W. Lu, C. Qian, H. Wang, L. Rao, T. Zeng, H. Liu, H. Liu, B. Fei, J. Hao, *Adv. Funct. Mater.* **2014**, *24*, 4051–4059.

[14] a) A. P. Vink, M. A. de Bruin, S. Roke, P. S. Peijzel, A. Meijerink, *J. Electrochem. Soc.* **2001**, *148*, E313–E320; b) C. Barthou, J. Benoit, P. Bennalloul, A. Morell, *J. Electrochem. Soc.* **1994**, *141*, 524–528.

[15] a) F. Wang, X. G. Liu, *J. Am. Chem. Soc.* **2008**, *130*, 5642 – 5643; b) F. Wang, X. G. Liu, *Chem. Soc. Rev.* **2009**, *38*, 976 – 989; c) F. Wang, Y. Han, C. S. Lim, Y. H. Lu, J. Wang, J. Xu, H. Y. Chen, C. Zhang, M. H. Hong, X. G. Liu, *Nature* **2010**, *463*, 1061 – 1065.
[16] A. Nag, S. Sapra, C. Nagamani, A. Sharma, N. Pradhan, S. V. Bhat, D. D. Sarma, *Chem. Mater.* **2007**, *19*, 3252 – 3259.
[17] a) F. Su, B. Ma, K. Ding, G. Li, S. Wang, W. Chen, A. G. Joly, D. E. McCready, *J. Lumin.* **2006**, *116*, 117 – 126; b) E. Song, W. Zhao, X. Dou, Y. Zhu, S. Yi, H. Min, *J. Lumin.* **2012**, *132*, 1462 – 1467.
[18] P. Wu, Y. He, H.-F. Wang, X.-P. Yan, *Anal. Chem.* **2010**, *82*, 1427 – 1433.
[19] J. Liu, L. Lu, A. Li, J. Tang, S. Wang, S. Xu, L. Wang, *Biosens. Bioelectron.* **2015**, *68*, 204 – 209.

Received: August 2, 2015
Published online: September 11, 2015

